Research Article | Vol. 10, No. 7 / 1 July 2020 / Optical Materials Express 1733
Optical Materials EXPRESS

# Supercontinuum generation in all-normal dispersion suspended core fiber infiltrated with water

TRUNG LE CANH,[1] VAN THUY HOANG,[1,2,3] HIEU LE VAN,[4] DARIUSZ PYSZ,[3] VAN CAO LONG,[5] THUAN BUI DINH,[1] DUNG TIEN NGUYEN,[1] QUANG HO DINH,[1] MARIUSZ KLIMCZAK,[2] RAFAŁ KASZTELANIC,[2,3] JACEK PNIEWSKI,[2] RYSZARD BUCZYNSKI,[2,3,*] AND KHOA XUAN DINH[1]

[1]*Department of Physics, Vinh University, 182 Le Duan, Nghe An Province, Vinh City, Vietnam*
[2]*Faculty of Physics, University of Warsaw, Pasteura 5, 02-093 Warsaw, Poland*
[3]*Department of Glass, Institute of Electronic Materials Technology, Wólczyńska 133, 01-919, Warsaw, Poland*
[4]*Institute of Research and Development, Duy Tan University, Da Nang 550000, Vietnam*
[5]*Institute of Physics, University of Zielona Góra, Prof. Szafrana 4a, 65-516 Zielona Góra, Poland*
[*]*ryszard.buczynski@fuw.edu.pl*

**Abstract:** Octave spanning all-normal dispersion supercontinuum generation (SCG) was experimentally demonstrated in a solid, suspended-core fiber (SCF) infiltrated with water. Replacement of air with water in the cladding air-holes leads to a dramatic modification of the dispersion profile of the fiber, significantly flattening the characteristic over the visible and much of the near-infrared wavelength range at normal values. In such a fiber infiltrated with water, all-normal dispersion supercontinuum was generated with the spectral coverage from 435 nm to 1330 nm using femtosecond pumping with the output peak power of 150 kW and 800 nm central wavelength. The SCF without water infiltration – air in the cladding region – had a zero-dispersion wavelength at 760 nm and enabled the generation of the anomalous dispersion dynamics-based SCG in the wavelength range from 450 nm to 1250 nm. We also numerically calculated the coherence of simulated supercontinuum pulses with one-photon-per-mode noise seeds and point out that the all-normal dispersion SCG in suspended-core fiber infiltrated with water has the potential for high temporal coherence, while the fiber without water infiltration shows gradual decoherence of generated supercontinuum pulses with increasing pump power, over similar peak power range.



## 1. Introduction

Supercontinuum generation (SCG), that is pulse broadening as a result of nonlinear optical phenomena in transparent materials, was first presented by Alfano and Shapiro in 1970 [1]. Afterwards, it has gained significant scientific interest due to possibility of SCG using photonic crystal fibers (PCFs), invented by Knight *et al.* in 1996 [2–4]. Supercontinuum sources that offer broad spectral bandwidth and high-power output have found applications, e.g. in metrology, telecommunication, spectroscopy, and pulse compression [5–7]. It is now a recognized and well-established technology with plenty of solutions, including commercial ones.

In the last years, different approaches for generation of broadband SCG spectra have been presented. Timmers *et al.* obtained an infrared spectrum with the wavelength range 4–12 µm based on intra-pulse difference frequency generation [8]. Optical fluoro-tellurite fibers based on soft glasses allow for SCG across visible (VIS) and mid-infrared (mid-IR) range as wide as 0.4–5 µm [9]. SCG in the range from near-IR up to 14 µm was obtained in fibers made of

#395936 https://doi.org/10.1364/OME.395936
Journal © 2020 Received 22 Apr 2020; revised 17 Jun 2020; accepted 18 Jun 2020; published 1 Jul 2020

Optical Materials EXPRESS

chalcogenide glass [10,11]. Introduction of liquids or gases into hollow-core fibers has also become a promising approach for SCG from ultra-violet (UV) to mid-IR [12–14].

However, most of SCG sources based on long-pulses (i.e. nanosecond order durations) are noise-driven and do not exhibit time coherence. The general, commonly applied method to obtain SCG is to use short pulses injected into nonlinear optical fibers. The central pulse wavelength is usually close to a zero-dispersion wavelength (ZDW), in the anomalous regime of dispersion. In such a case and when femtosecond pulses are used at input, SCG bandwidth is broadened rapidly by soliton dynamics and here another decoherence mechanism can come into play, in particular, related to breakup of the input pulse due to soliton fission. Any small intensity fluctuations of resulting fundamental solitons give rise to wavelength fluctuations through Raman soliton self-frequency shift (SSFS). They are then transferred into time domain, because supercontinuum pulses experience chromatic dispersion as they propagate in a fiber. As a consequence, anomalous dispersion-pumped SCG pulses are characterized by a complex temporal profile, considerable intensity variations, and low coherence (spectrally resolved modulus of the complex degree of first-order coherence at zero path difference) [4,15].

A typical approach for temporally coherent SCG is to use femtosecond laser pulses launched into all-normal dispersion (ANDi) fibers to mitigate the noise and to improve the temporal coherence characteristics. Difficulties in this field are related to the fact that much higher peak power of pulses is required than in the case of modulation instability- or soliton fission-based SCG [16].

To this day several solutions have been reported for broadband ANDi SCG. For example, soft glass fibers made from chalcogenide or telluride glasses have been used, since these glasses have high nonlinearity and normal material dispersion up to mid-IR [12,17–19]. However, it is challenging to design a fiber with near-zero flat normal dispersion, because highly negative material dispersion of these glasses dominates. Moreover, soft glasses are mechanically weak and tend to crystalize what makes the development of complex structures problematic [20].

Among silica fibers, a number of solutions for ANDi SCG, using different fiber types, have been proposed in the last years, which is summarized in Table 1. The main drawback of silica, besides the limited transmission in IR, is relatively low nonlinearity. Since the nonlinear coefficient $\gamma$ is inversely proportional to the effective mode area, small-core silica fibers are required to achieve an efficient SCG, as a general rule.

**Table 1. State-of-the-art experimental results for all-normal dispersion SCG in silica fibers.**

| Fiber type | Pulse duration [fs] | Pump wavelength [nm] | Peak power [kW] | Spectral bandwidth [nm] | Ref. |
|---|---|---|---|---|---|
| step-index | 110 | 1690 | 20 | 1100–2100 | [40] |
| step-index | 712 | 1552 | 16 | 1400–1725 | [41] |
| polarization-maintaining | 229 | 1041 | 23 | 750–1300 | [42] |
| PCF | 50 | 650 | 22 | 425–900 | [43] |
| | | 790 | 250 | 540–1420 | |
| | | 1050 | 156 | 600–1500 | |
| PCF | 350 | 1064 | 114 | 700–1400 | [44] |
| PCF | 3800 | 1055 | 1 | 930-1230 | [16] |
| PCF | 125 | 1550 | 9 | 1340-1820 | [45] |
| PCF | 170 | 1064 | 50 | 750-1400 | [46] |
| | 235 | 1064 | 35 | 750-1350 | |
| silicate PCF | 500 | 1550 | 130 | 975-2075 | [47] |
| suspended-core tapered | 50 | 625 | 26 | 370–895 | [48] |

Optical Materials EXPRESS

A promising approach is to use suspended core fibers (SCFs) that are fibers composed of small cores, suspended on thin glass bridges [21]. In these fibers, the light is strongly confined in the core what results in high $\gamma$ [22]. A number of papers presenting SCG in silica and soft glasses-based SCFs have been published [23–26], although the control of dispersion and the possibility to achieve all-normal dispersion regime in SCFs is limited [27,28].

Several works related to fibers infiltrated with liquids for ANDi SCG have been presented. With high nonlinearity of liquids, the liquid-core fibers offer broad ANDi SCG [29–34]. Another idea is to use liquids filling air-holes in the photonic cladding to modify dispersion of PCFs. Both numerical and experimental results were reported [35,36].

Possibility of using SCFs infiltrated with liquids for SCG has also been considered [37–39]. In the work by Xuan *et al.*, a theoretical possibility of dispersion modification in SCFs was analyzed [38]. They showed that filling the air-holes with water can change a typical SCF dispersion characteristic into all-normal near-zero flat dispersion characteristic in the wavelength range 700–1500 nm, for a core diameter of 1.32 µm. In the paper by Sharafali *et al.* numerical analysis of a suspended liquid-core (filled with carbon tetrachloride) fiber for SCG with femtosecond pump laser was presented [39]. This fiber offers octave-spanning SCG with as low input peak power as 5 kW.

In this paper, we verify the above concept experimentally. We compare the dispersion characteristics of a similar SCF developed in-house with the cladding holes containing air and the same SCF with the holes filled with water. Next, we test the possibility and the properties of SCG in both fibers. We also numerically calculate the coherence characteristics of SCG in these fibers and anticipating that ANDi SCG in SCFs infiltrated with water would have the potential for high coherence. We use water because in spite of high absorption and low nonlinearity it has properties that are crucial for splicing SCFs with standard fibers to build all-fiber systems. Water is non-flammable, non-toxic and its evaporation rate is lower than for popular solvents used in PCFs. Since only a small portion of the guided mode is located in water the guided mode loss is still low and we do not exploit the nonlinearity of water, but use water to change the dispersion characteristic.

## 2. Development of SCF

First, we numerically studied the influence of the core diameter $d_{\mathrm{core}}$ on the fundamental mode dispersion characteristic in SCFs using the commercial software Lumerical MODE based on the finite-difference eigenmode method [49]. A structure with three air-holes in the cladding has been assumed in the simulations. Material dispersion and attenuation of water were employed after Ref. [50].

Figure 1 shows the dispersion profile of SCFs with different $d_{\mathrm{core}}$. In the case of unfilled SCFs, the increase of $d_{\mathrm{core}}$ leads to a shift of ZDWs towards long wavelengths. When $d_{\mathrm{core}}$ changes from 1.3 µm to 1.7 µm, ZDW shifts from 685 to 755 nm. For the water-filled SCFs, the increase of $d_{\mathrm{core}}$ results in blue-shifting of ZDW. For $d_{\mathrm{core}}$ = 1.6 µm and 1.7 µm, their ZDWs are 1010 nm and 1100 nm, respectively, and thus, these fibers are not suitable for ANDi SCG. The fiber with $d_{\mathrm{core}}$ = 1.3 µm has ZDW at 1650 nm, while for $d_{\mathrm{core}}$ = 1.45 ZDW equals 1450 nm. However, in the case of a sub-micron $d_{\mathrm{core}}$, obtaining high coupling efficiency is a challenge.

The selected silica SCF was developed using the standard stack-and-draw method [51]. In the first step, a triangle-shaped preform consisting of 3 central capillaries and 120 rods made of silica (Ohara SK-1310) has been stacked. Diameters of the capillaries and the rods were 0.92 mm. Next, the preform has been embedded in an outer tube and drawn using a standard drawing tower to form a subpreform with the diameter approx. 3 mm. The subpreform has fully integrated structure with 3 holes surrounding a small core. From this subpreform the final fiber was drawn. To achieve the suspended core structure with large holes and thin glass bridges, pressure to the

Optical Materials EXPRESS

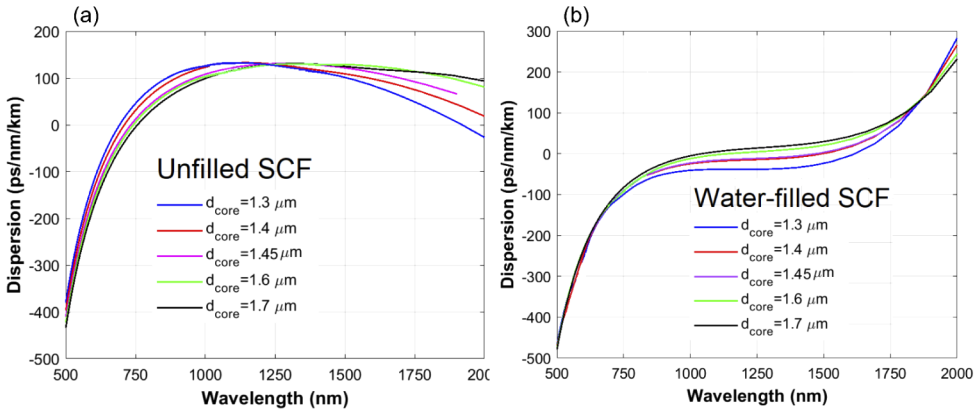


**Fig. 1.** Numerically obtained dispersion characteristics with various $d_{\text{core}}$ for (a) unfilled SCF and (b) water-filled SCF.

subpreform has been applied. The final fiber diameter was in the range 120–125 µm. As shown in Fig. 2, the thickness of the bridges $t$ is approx. 106 nm, while the core diameter $d_{\text{core}}$ is 1.47 µm.

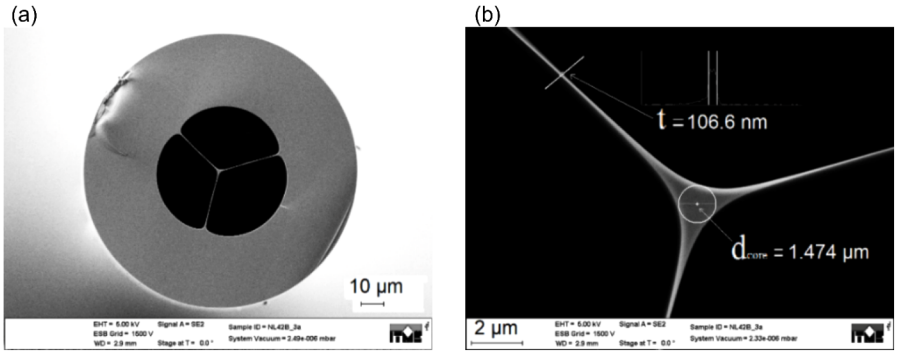


**Fig. 2.** Scanning electron microscope (SEM) images of the developed SCFs.

The fiber with air-holes was labeled #$F_1$, and the fiber with the holes infiltrated with water was labeled #$F_2$.

The liquid pumping system with a standard syringe pump New Era Pump System NE-300 was used to infiltrate the SCF with distilled water. The pump was connected to the custom-made metal reservoir with SCF mounted in the reservoir's wall, as shown in Fig. 3. The metal reservoir is fully filled with water, and the water is pumped at a continuous infusion rate 2 µL/min. The infiltration of a 60 cm–long fiber sample takes about 1 minute.

The evaporation of water is negligible if measurements are performed with fiber samples of lengths of tens of centimeters and within few days. Additional measurements of SCG after 1 h, 24 h, 48 h, 72 h, and 120 h, have shown that the spectral width of SCG is maintained within the dynamics of 5 dB and the intensity of SCG lowers by approx. 5 dB during at least 72 hours, while after that time the structure and the width of SCG changes. If the fiber is expected to work for longer than 72 h the reservoir should be used for continuous water refilling, what comes at a cost of lower coupling efficiency and system complexity. In such a case we achieved in our experiment the coupling efficiency of 17% a 40× objective was used (Newport M-40X) and 10% for the objective 10× (Newport M-10X).

Optical Materials EXPRESS

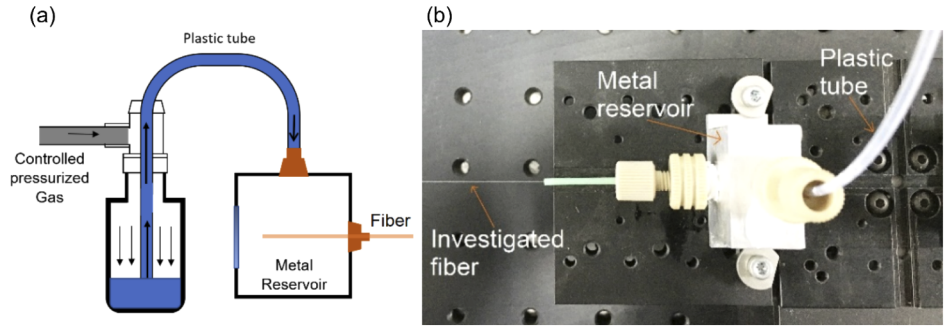


**Fig. 3.** (a) Schematic of the pump system used to infiltrate SCF with water, (b) a photograph of the fiber and metal reservoir.

The dispersion characteristics of $\#F_1$ and $\#F_2$ were verified using a setup based on Mach-Zehnder interferometer, as shown in Fig. 4. Koheras SuperK, emitting white-light in the range 450–2400 nm, was used as a source. The source beam is collimated by the micro-objective $MO_1$ and then divided into two beams by the 50/50 beam splitter $BS_1$. The signal beam is coupled into the investigated fiber using the micro-objective $MO_2$. The output beam from this fiber is collimated by the micro-objective $MO_3$ and then changes the direction by the use of the mirror $M_1$. Next, this beam propagates toward the beam splitter $BS_2$. The intensity of the reference beam is controlled by the variable neutral density filter NDF. The length of the optical path in this arm is controlled by the translational stage containing the mirrors $M_3$ and $M_4$ that are mounted on a micro-positioner. The positions of these mirrors and the corresponding spectral signals are recorded. All the components, i.e., micro-objectives, variable intensity filters, etc., were characterized and their influence on the dispersion measurement of the fiber have been taken into account. The interference fringes were recorded using the VIS spectrometer Ocean Optics Red Tide with the wavelength range 350–1000 nm and the IR spectrometer Avantes AvaSpec-NIR256/512-1.7 with the wavelength range 900–1700nm.

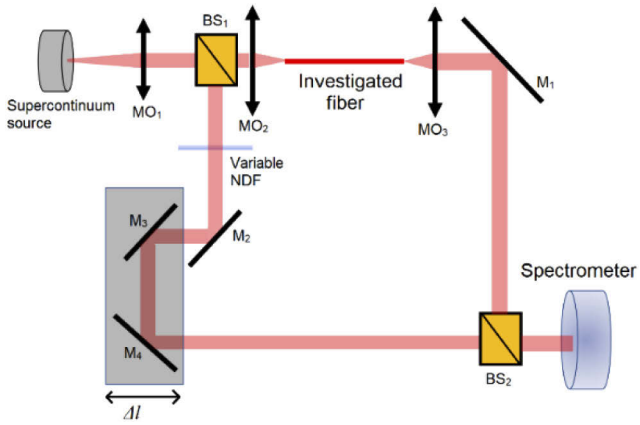


**Fig. 4.** Schematic representation of the Mach-Zehnder interferometer system to measure dispersion characteristics of the investigated fibers.

The dispersion characteristics of $\#F_1$ and $\#F_2$, obtained experimentally and from the numerical simulations, are shown in Fig. 5. The experimental results are in good agreement with the numerical data. They confirm that $\#F_1$ has anomalous dispersion in the near-IR range and ZDW around 760 nm (Fig. 5(a)). The dispersion value changes from –400 to 140 ps/nm/km

Optical Materials EXPRESS

in the wavelength range 500–1300 nm. The fiber #$F_2$ has normal dispersion in the visible and the near-IR range and ZDW at 1400 nm. The dispersion profile of #$F_2$ is flatter than that of #$F_1$ in the near-IR range. The dispersion values of #$F_1$ vary from –50 to 140 ps/nm/km in the wavelength range 680–1300 nm, while the dispersion of #$F_2$ changes from –50 to 50 ps/nm/km in the wavelength range 820–1720nm.

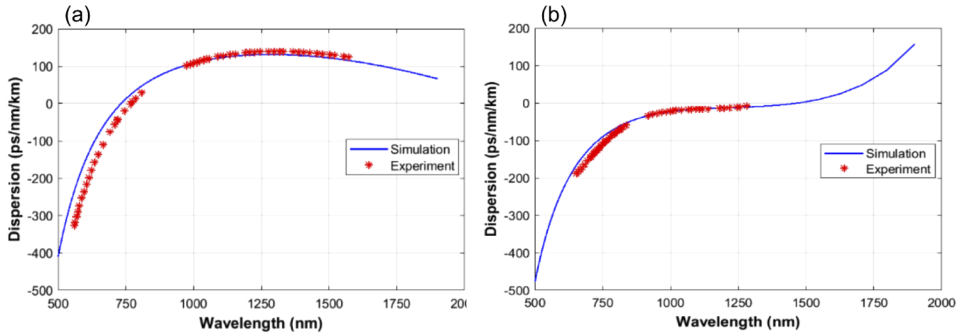


**Fig. 5.** Dispersion characteristics obtained numerically and experimentally, (a) #$F_1$, (b) #$F_2$.

With the anomalous dispersion profile #$F_1$ enables soliton-fission-driven SCG of low coherence, while #$F_2$ can provide SCG in all-normal dispersion regime, with flat spectrum and high potential for temporal coherence.

The loss of the investigated fibers was measured using the cut-back method. The schematic of the method is shown in Fig. 6. The white-light emitted from SCG source in the wavelength range 450–2400 nm is collimated by the micro-objective $MO_1$ and then coupled into the fibers using the micro-objective $MO_2$. The output light from the fibers is collected by a commercial multimode fiber integrated with a spectrometer. We used the optical spectrum analyzer YOKOGAWA-AQ6370D in the wavelength range of 600–1700nm and the spectrometer Ocean Optics Red Tide in the wavelength range 350–1000 nm. The losses $L$ are calculated according to equation

$$L = \frac{10}{l_1} \cdot \log \frac{P_2}{P_1}, \tag{1}$$

where $l_1$ denotes the length of the cut-off fiber section, $P_1$ and $P_2$ are the output powers for the long and short fiber samples, respectively. In this setup, $l_1 = 110$ cm and 36 cm, for #$F_1$ and #$F_2$, respectively.

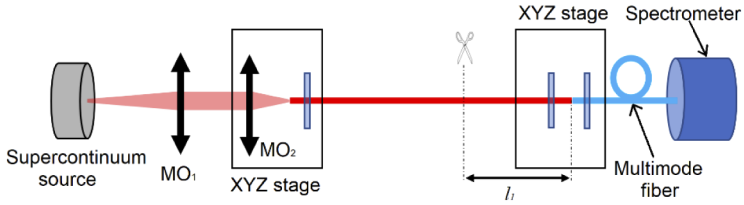


**Fig. 6.** Schematic of the setup used to measure the losses in the investigated fibers.

Measured attenuation characteristics of the investigated fibers are shown in Fig. 7. The fiber #$F_1$ has losses approx. 4 dB/m in the visible and near-IR wavelength range. For longer wavelengths the loss is higher and reaches the maximum of 9 dB/m at approx. 1350 nm. The losses of #$F_2$ are higher than that of #$F_1$ in almost entire analyzed spectrum, with two main peaks reaching approx.

Optical Materials EXPRESS

18 dB/m, at 960 nm and 1150 nm. The higher loss of #$F_2$ relates to high attenuation of water in the air-holes. In such a case the mode is less confined in the silica core, and a larger fraction of the light energy propagates in the water cladding. However, with the small $d_{core}$ and the resulting small mode area $A_{eff}$ the fiber #$F_2$ has still high nonlinear coefficient γ, which allows for SCG with broad spectral bandwidth in few centimeters-long propagation lengths. Therefore, the losses of this fiber do not reduce the spectral broadening significantly.

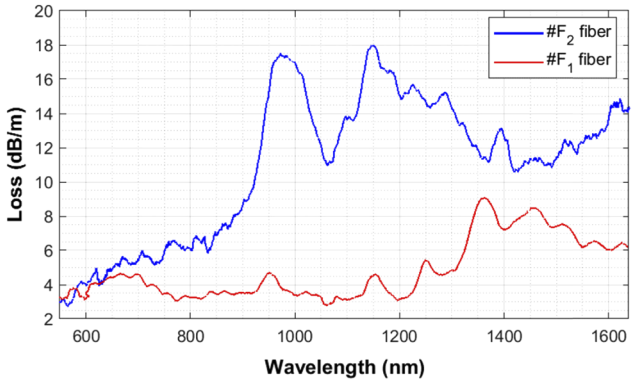


**Fig. 7.** The losses in the analyzed fibers as a function of the wavelength.

Due to the infiltration of water into the air-holes, the contrast of the refractive index between the core and the cladding of #$F_2$ is smaller than that of #$F_1$. Therefore, with the same $d_{core}$ the fiber #$F_2$ has larger $A_{eff}$ than #$F_1$. As shown in Fig. 8, $A_{eff}$ of #$F_1$ increases from 1.4 μm$^2$ for the wavelength 400 nm to 2.3 μm$^2$ for the wavelength 1500 nm, while of #$F_2$ increases from 1.62 μm$^2$ to 4.1 μm$^2$. The nonlinear coefficient γ of the investigated fibers is calculated according to Eq. (2), where $n_2$ is the nonlinear refractive index of silica ($n_2 = 2.74\times10^{-20}$ m$^2$/W at 1064 nm [52]):

$$\gamma = \frac{2\pi}{\lambda}\frac{n_2}{A_{eff}}. \tag{2}$$

Figure 8 shows γ of #$F_1$ and #$F_2$. The fiber #$F_1$ has γ from 155 W$^{-1}$km$^{-1}$ to 94 W$^{-1}$km$^{-1}$ when the wavelength changes from 400 nm to 1500 nm, while #$F_2$ – from 132 W$^{-1}$km$^{-1}$ to 52 W$^{-1}$km$^{-1}$.

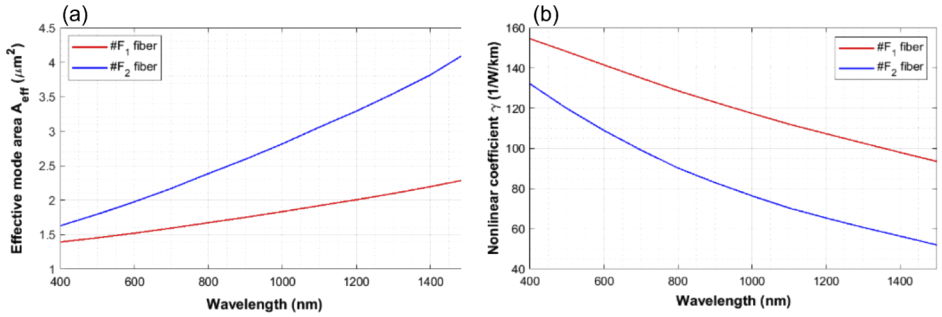


**Fig. 8.** Numerically calculated (a) effective mode area $A_{eff}$ and (b) nonlinear coefficient γ for the investigated fibers.

Optical Materials EXPRESS

## 3. SCG in the developed fibers

SCG in the developed fibers was analyzed using a setup shown in Fig. 9. The pump source was a Ti:Sapphire femtosecond solid-state oscillator ATSEVA LLC TIF-SP with the following parameters: pulse duration 28 fs, central wavelength 800 nm, repetition rate (80 ± 10) MHz, and average output power 687 mW that corresponds to peak power of 510 kW. The input beam was coupled into the investigated fibers using a 40× microscope objective $MO_1$. The output beam was collected with a 10× microscope objective $MO_2$ and directed into a large core multimode fiber integrated with a spectrometer. We used an optical spectrum analyzer YOKOGAWA-AQ6370D (range 600–1700nm), and Czerny-Turner compact spectrometer Ocean Optics Red Tide (range 350–1000 nm) to record the SCG spectra. The coupling efficiencies were also measured: 20% and 30% for $\#F_1$ and $\#F_2$, respectively. The length of $\#F_1$ and $\#F_2$ used in this part of the experiment was 12 cm.

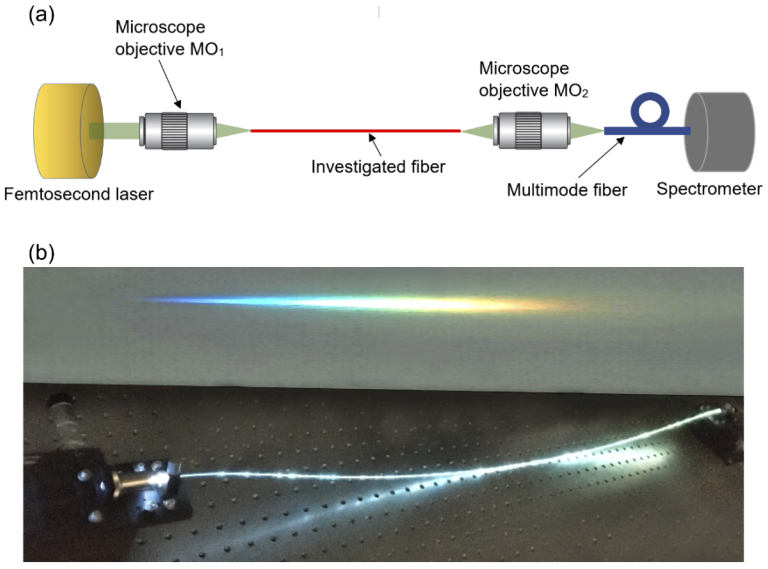


**Fig. 9.** (a) Schematic of the setup used to measure SCG spectra in the investigated fibers, (b) a photograph of the all-normal supercontinuum generated in $\#F_2$, dispersed by a grating and projected onto a screen.

The fibers $\#F_1$ and $\#F_2$ are multimode at $\lambda = 800$ nm. In particular, based on numerical analysis, $\#F_1$ can guide 7 modes while $\#F_2$ can guide 3 modes. However, in our setup single-mode operation is achieved by adjusting the coupling. Figure 10(a) shows the far-field optical image of the output beam $\#F_2$ made with a CCD camera. The radial beam intensity distribution with the fitted Gaussian profile is shown in Fig. 10(b). The good agreement between the experimental data and the fitted curve confirms the single-mode operation of the fiber.

We also numerically modelled SCG in the investigated fibers to verify the experimental results and to analyze the nonlinear processes responsible for spectral broadening. In order to achieve these goals we solved the general nonlinear Schrodinger equation (GNLSE) in the frequency domain [4], and GNLSE used here is given in the following form:

$$\partial_z \tilde{A} - \sum_{k\geq 2} \frac{i^{k+1}}{k!} \tilde{\beta}_k(z) \frac{\delta^k A}{\delta t^k} + \frac{\tilde{\alpha}(\omega)}{2} \tilde{A} = i\gamma \left(1 + \frac{\omega - \omega_0}{\omega_0}\right) \tilde{A} \mathcal{F} \left[ \int_{-\infty}^{\infty} R(T') |A(T - T')|^2 dT' \right] \quad (3)$$

where $\tilde{A}(z, \omega)$ is Fourier transform of the amplitude of a pulse $A(z, T)$, and $R(T)$ is Raman response function.

Optical Materials EXPRESS

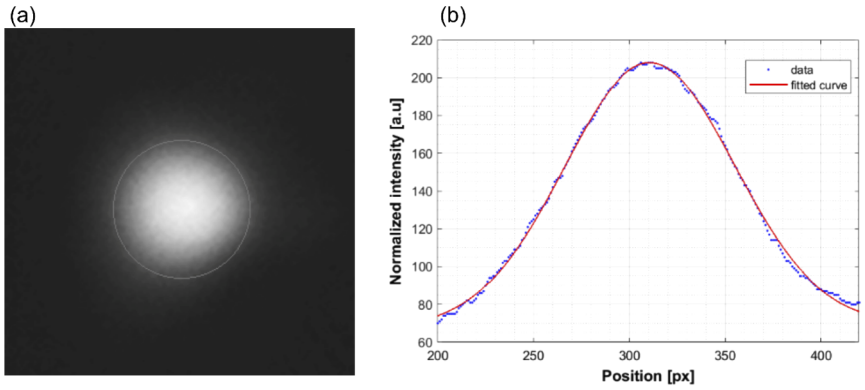


**Fig. 10.** (a) The far-field optical image of the output beam emitted from #$F_2$, (b) radial intensity distribution of the central section of the image compared to the Gaussian function profile.

The left side of Eq. (3) describes linear propagation effects with $\tilde{\alpha}$ and $\tilde{\beta}$ related to attenuation and dispersion of the fiber, respectively. These linear parameters were obtained in the experimental analysis of the linear properties of the fibers and were shown in Fig. 5 and Fig. 7.

The right side of the equation models nonlinear effects, which depend on the nonlinear properties of silica. The term $\gamma(\omega)$ stands for frequency-dependent nonlinear coefficient and this characteristic is shown in the wavelength scale in Fig. 8. Nonlinear response function $R(T)$ consist of instantaneous part originated from the electronic bound contribution and the non-instantaneous contribution induced by molecular vibrations

$$R(T) = (1 - f_R)\delta(T) + f_R h_R(T), \tag{4}$$

where $f_R = 0.18$ is the fractional contribution of delayed Raman response, $\delta(T)$ is Dirac delta function, $h_R(T)$ represents the retarded response [53,54].

The form of $h_R(T)$ is defined from the experimental data and is given according to equation

$$h_R(T) = \frac{\tau_1^2 + \tau_2^2}{\tau_1 \tau_2^2} \exp\left(\frac{-T}{\tau_2}\right) \sin\left(\frac{T}{\tau_1}\right) \Theta(T), \tag{5}$$

where $\Theta(T)$ is Heaviside step function, $\tau_1 = 12.2$ fs, and $\tau_2 = 32$ fs [53,54].

Temporal coherence of SCG is determined by using the first-order coherence in the form [3]

$$|g_{12}^{(1)}(\lambda, t_1 - t_2 = 0)| = \left| \frac{E_1^*(\lambda, t_1) E_2(\lambda, t_2)}{[|E_1(\lambda, t_1)|^2 |E_2(\lambda, t_2)|^2]^{1/2}} \right|, \tag{6}$$

where angle brackets denote ensemble average over independently generated pairs of SCG spectra [$E_1$, $E_2$] with one-photon-per-mode noise seeds. Here, we apply a noise model, in which the input shot noise is modelled by addition of one photon with random phase per each simulation bin ("one photon per mode"). In addition to that, we account for the intensity fluctuations of the input pulse amplitude modelled with relative intensity noise (RIN) which was 0.1% (integrated RIN, provided in the laser specification sheet). Our implementation of noise modelling follows the formalism recently proposed by Genier et al. [55]. We note that the one photon per mode noise model describes vacuum noise and is distinct from modulation instability decoherence [56].

In SCG simulations, we used one polarization model. The interaction between two polarization modes will degrade the coherence of SCG spectrum. However, with the short pulse duration of the input pulse, the polarization noise can be neglected [46].

Optical Materials EXPRESS

The experimental results of SCG in #$F_1$ for various measured fiber output powers are shown in Fig. 11(a) with solid traces. The length of the fiber was 12 cm. With the maximum output power 40 mW SCG spectrum spanned the range 450–1300 nm within 20 dB dynamic range. For the average output power 20 mW, the prominent features of the broadened spectrum include a red-shifted soliton with the central wavelength of approximately 1100 nm and a dispersive wave centered around 550 nm. Red-shifting of the soliton, accompanied by blue-shifting of the dispersive wave can be observed for the increasing pump power (corresponding to the increase of the observed output power).

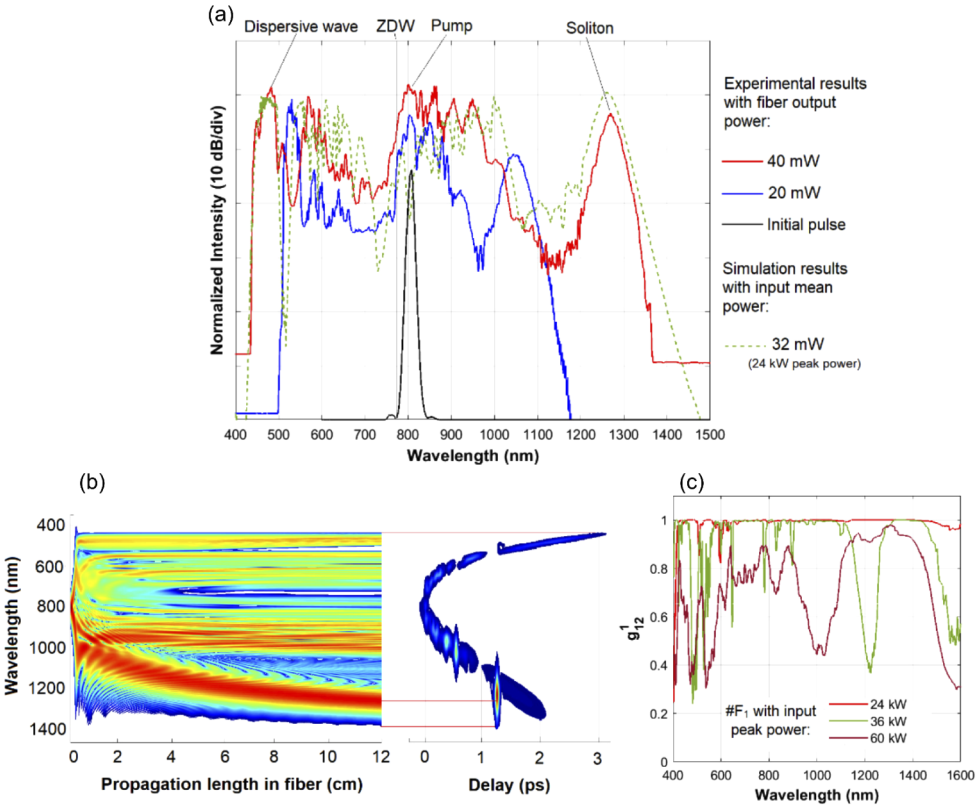


**Fig. 11.** (a) Experimentally obtained SCG spectra for various fiber output average powers and numerically simulated SCG spectra for the input peak power 24 kW for reference. (b) Numerically simulated pulse evolution in #$F_1$ with input peak power 24 kW and the spectrogram of the output beam at 12 cm of propagation. (c) Coherence degree obtained from 20 individual pairs of pulses with input noises and various input peak powers, for #$F_1$.

The numerical results of SCG in #$F_1$, shown in Fig. 11(a) with dashed lines, were calculated for the pulse duration 28 fs and the propagation length of 12 cm. Influence of the microscope objective for pulse broadening is neglected in our modelling since optical pathway in glass is very short and it does not influence significantly on pulse length in our case. The peak power at the input end of the fiber was assumed 24 kW, that matched the bandwidth of experimentally obtained spectra with the average recorded output powers around 40 mW. The structure of simulated SCG spectrum is different from the experimental one, and the input average power in simulation (32 mW) is smaller than the actual power (approx. 43 mW).

We speculate that these discrepancies relate to the multimode operation of #$F_1$. Moreover, the interaction between these modes leads to the energy transfer from the fundamental mode

Optical Materials EXPRESS

into high-order modes, resulting in a reduction of the spectral bandwidth and in a change of the structure of the output spectrum [57]. In addition to that, modulation instability at this peak power level is also related to the appearance of some fine structure differences between the simulated and measured supercontinuum spectra. This postulation is also supported by the evolution of the computed degree of coherence of the generated SCG pulses, discussed in the following section. When only the fundamental mode is excited, the high input peak power offers the high number of solitons and soliton fission will occur at short propagation in the fiber. The soliton-red shifting accompanied by a dispersive wave still plays the main role for spectral broadening at the edges of the pulse. However, the input noise is also strongly amplified resulting in degradation of temporal coherence of the SCG spectrum.

Figure 11(b) (left panel) shows pulse evolution in $\#F_1$ during propagation, for the input peak power 24 kW, the pump wavelength 800 nm, and the pulse duration 28 fs. At the beginning, self-phase modulation (SPM) is the main contribution to the broadening dynamics. Soliton fission appears at 4 mm of propagation. This is followed by soliton self-frequency shift (SSFS) at the red-shifted wavelengths of SCG spectrum, which corresponds to the leading edge of the pulse in the anomalous dispersion, while the dispersive waves, extending into the visible wavelengths, can be observed at the trailing edge of the pulse. Figure 11(b) (right panel) shows the computed pulse spectrogram at 12 cm of propagation. It takes a specific concave shape with red-shifting solitons and blue-shifted dispersive waves, which is in agreement with the concave dispersive characteristic of the fiber, shown in Fig. 5(a).

For the estimation of coherence properties, characteristic lengths of pulse broadening dynamics in $\#F_1$ were calculated, using the following set of formulas:

$$L_D = \frac{t_0^2}{|\beta_2|},\ L_{NL} = \frac{1}{\gamma P_0},\ N = \sqrt{\frac{L_D}{L_{NL}}},\ L_{fiss} = \frac{L_D}{N},\ L_{MI} \approx 16 L_{NL}, \tag{7}$$

where $L_D$, $L_{NL}$, $L_{fiss}$, $L_{MI}$ are dispersive, nonlinear, soliton fission, and MI characteristic length scales, respectively. $N$ is soliton number, $P_0$ and $t_0$ are peak power and pulse duration of an input pulse (equal 28 fs). The parameter $\beta_2$ represents the group velocity dispersion at the central wavelength of the input laser pulse. For $\#F_1$, $\beta_2 = -0.0146$ ps$^2$/m, $\gamma = 129$ W$^{-1}$·km$^{-1}$. Furthermore, we put the characteristic length scale analysis into the context of coherence properties of SCG generated in $\#F_1$. Figure 11(c) shows the calculated first-order degree of coherence of the anomalous dispersion-pumped SCG with various input peak powers. The coherence level of anomalous dispersion SCG significantly depends on relative length scales associated with the processes of MI and soliton fission. In the case of the input peak power 24 kW, that corresponds to $L_D = 5.4$ cm, $L_{NL} = 0.032$ cm, $N \approx 12$, $L_{fiss} = 0.42$ cm, $L_{MI} = 0.52$ cm. According to these calculations, soliton fission occurs not long before the onset of MI-related noise which corresponds to the coverage of the MI gain bands with seed signal, which has not experienced significant decoherence due to soliton dynamics. As a result, the supercontinuum pulses obtained for the lowest considered peak power 24 kW are associated with high degree of coherence, which is in agreement with the earlier numerical and experimental studies [3,58–60]. The increase of the input peak power leads to the reduction of MI length scale, which is proportional to the reciprocal of peak power through the term $L_{NL}$. For instance, the input peak power 60 kW corresponds to $L_{NL} = 0.02$ cm, $N \approx 16$, $L_{fiss} = 0.26$ cm, $L_{MI} = 0.21$ cm. The amplification of the input noise by MI would occur before the process of soliton fission in this case [3]. Consequently, a gradual decoherence with the increasing peak power of the simulated SCG is observed for 36 kW and 60 kW peak power. These results also support our earlier postulation that the increasing structuring of SCG spectra obtained experimentally is caused by the increasing significance of MI in the broadening dynamics and not by the jitter introduced by SSFS of fundamental solitons.

Optical Materials EXPRESS

An entirely different SCG dynamics is expected in #$F_2$ with normal dispersion characteristic over much of the wavelength range of the interest in this study. The SCG spectra recorded in #$F_2$ with various output average powers are shown in Fig. 12(a). The length of the fiber was 12 cm. With the maximum output power 160 mW, the output spectrum spanned the wavelength range 435–1330 nm within 20 dB dynamic range. The numerical results of SCG in #$F_2$, shown with the dashed line in Fig. 12(a) were calculated with pulse duration 28 fs, propagation length 12 cm and the input peak power 150 kW.

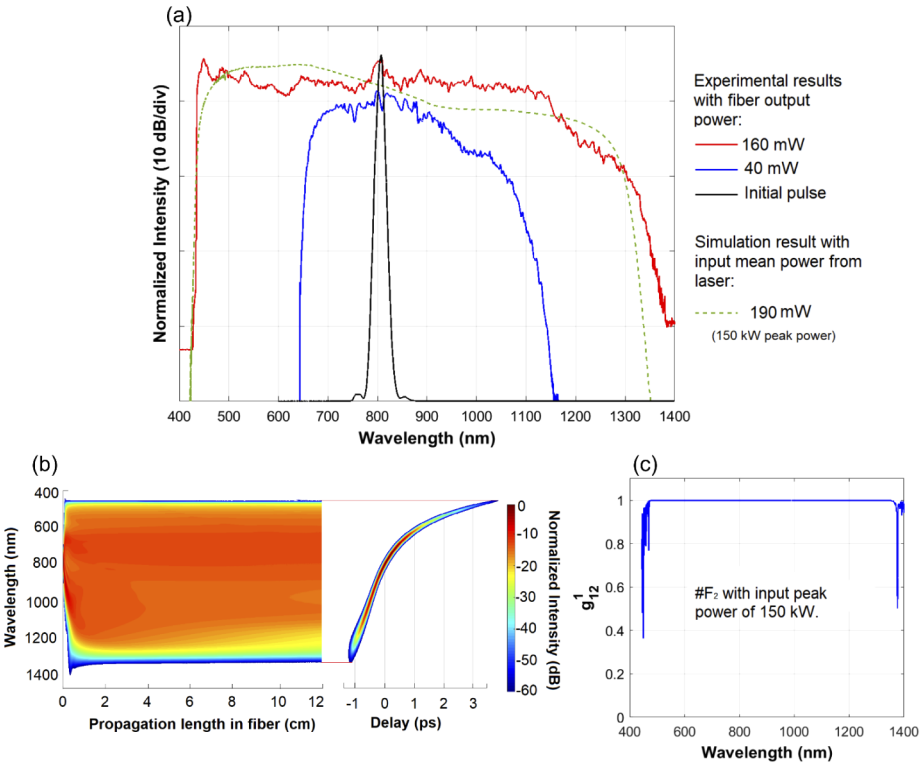


**Fig. 12.** Experimentally obtained SCG spectra for various fiber output powers and the numerically simulated SCG spectra with the input peak power 150 kW, for #$F_2$. (b) Numerically simulated pulse evolution in #$F_2$ with the input peak power 150 kW and the spectrogram of the output beam at 12 cm of propagation. (c) Coherence degree obtained from 20 individual pairs of the pulses with input noises and peak power 150 kW, for #$F_2$.

The evolution of pulses during propagation in #$F_2$ is shown in Fig. 12(b) (left panel). At the beginning of propagation, SPM is the main contribution to the spectral broadening. Optical wave breaking (OWB) occurs first on the trailing pulse edge at 0.2 cm of propagation and gives rise to a new wavelength band extending into the short wavelengths up to 435 nm. At the leading of the pulse, OWB occurs at 3 cm of propagation with a new wavelength band generated around 1300 nm. During further propagation, the spectral broadening at the trailing edge of the pulse is inhibited by the high slope of the dispersion profile. At the leading edge, there is the potential for further spectral broadening. However, the limitation here relates to the increase of $A_{eff}$ at the long wavelengths resulting in the decrease of the fiber nonlinear response $\gamma$. Figure 12(b) (right panel) shows the spectrogram of the pulse at 12 cm of propagation. The stretching of this trace in the time domain with positive values of delay between around 1–3 ps corresponds to a situation, when the pulse stretches in the time domain due to dispersion, but this is not

Optical Materials EXPRESS

accompanied by a further increase of the spectral width. The reason for this phenomenon is that the adjacent spectral components overlap in time for too short period to contribute effectively to further spectral broadening. The numerical analysis of first-order degree of coherence of the simulated SCG pulses with the input peak power of 150 kW was calculated with 20 individual pairs with different random noise seeds. The obtained degree of coherence characteristic is shown in Fig. 12(c) and allows to anticipate high coherence of the supercontinuum pulses obtained in $\#F_2$ over the entire spectral width.

## 4. Conclusions

We experimentally investigated SCG in two SCFs. One is a fiber with the air-holes in the cladding. The second one is the same fiber but with the holes in the cladding filled with water. We confirmed that infiltration with water shifts ZDW to 1400 nm that allows for ANDi SCG under pumping with a femtosecond laser delivering 28 fs–long pulses centered at a wavelength 800 nm. The SCG spectrum covered the wavelength range 435–1330 nm within 20 dB dynamic range, when the input peak power 150 kW is applied. This peak power level corresponds to the pump pulse energy of just 2.5 nJ, covering the entire visible wavelength range with flat spectrum of coherent laser pulses. We also measured anomalous dispersion-pumped SCG in the same fiber without water infiltration. The obtained spectral bandwidth extended from 450 nm to 1300 nm.

With the unique properties of liquids, e.g., real-time dispersion modification, the use of SCFs with liquid infiltration is a viable approach for SCG applications in the range from ultra-violet to the near-IR wavelength range.

The presented setup for SCG is a proof-of-concept. Our primary goal is to achieve SCG in fibers that can be spliced with standard optical fibers to create an all-fiber system. In our experiments we have used a femtosecond Ti:Sapphire laser as a highly efficient laboratory source for testing novel fibers, but in target system it can be replaced with fiber femtosecond laser. After splicing, an all-fiber system does not require re-filling with water. We are also aware that splicing liquid-filled SCFs with other fibers is challenging. However, local evaporation of liquid in the close vicinity of a splice does not influence the dispersion characteristic or guiding properties in case of a solid core, which is the case of suspended core fibers.

Compared to octave-spanning ANDi SCG in the previous works in Refs. [42,43], the use of SCF with a small core allows to obtain a broad normal-dispersion SCG with the pump peak power limited to the kW range. The peak power used in [43] was about 250 kW, corresponding to a pulse energy 12.5 nJ, while the input pulse energy in our work is 2.5 nJ (peak power of 150 kW). The water-filled SCF fiber can offer broad ANDi SCG with further lower input peak power when the laser source with longer central wavelength is used.

The peak power used in this work is higher than that in Ref. [48]. However, a tapered SCF used by the authors, which has all-normal dispersion in visible and NIR range, was suited for low pulse energies around 1 nJ (peak power of 20 kW) due to pulse distortions over the adiabatic transition section of the taper occurring at higher pulse energies. The SCF structure infiltrated with water allowed to work around this bottleneck, yielding similar spectral coverage and increased output power level. Importantly, light sources with such characteristics have played significant roles in applications that demanded high photon flux [7].

## Funding

Fundacja na rzecz Nauki Polskiej (POIR.04.04.00-1C74/16); Narodowe Centrum Nauki (UMO-2016/21/M/ST2/00261); Uniwersytet Warszawski (statutory research); Ministry of Science and Technology (DTDL.CN- 32/19).

Optical Materials EXPRESS

## Disclosures

The authors declare no conflicts of interest.

## References


1. R. R. Alfano and S. L. Shapiro, "Emission in the region 4000 to 7000 Å via four-photon coupling in glass," Phys. Rev. Lett. **24**(11), 584–587 (1970).
2. J. C. Knight, T. A. Birks, P. S. J. Russell, and D. M. Atkin, "All-silica single-mode optical fiber with photonic crystal cladding," Opt. Lett. **21**(19), 1547–1549 (1996).
3. J. M. Dudley, G. Genty, and S. Coen, "Supercontinuum generation in photonic crystal fiber," Rev. Mod. Phys. **78**(4), 1135–1184 (2006).
4. J. M. Dudley and J. R. Taylor, *Supercontinuum Generation in Optical Fibers* (Cambridge University Press, 2010).
5. R. R. Alfano, "The ultimate white light," Sci. Am. **295**(6), 86–93 (2006).
6. J. T. Woodward, A. W. Smith, C. A. Jenkins, C. Lin, S. W. Brown, and K. R. Lykke, "Supercontinuum sources for metrology," Metrologia **46**(4), S277–S282 (2009).
7. C. R. Petersen, P. M. Moselund, L. Huot, L. Hooper, and O. Bang, "Towards a table-top synchrotron based on supercontinuum generation," Infrared Phys. Technol. **91**, 182–186 (2018).
8. H. Timmers, A. Kowligy, A. Lind, F. C. Cruz, N. Nader, M. Silfies, G. Ycas, T. K. Allison, P. G. Schunemann, S. B. Papp, and S. A. Diddams, "Molecular fingerprinting with bright, broadband infrared frequency combs," Optica **5**(6), 727–732 (2018).
9. D. D. Hudson, S. Antipov, L. Li, I. Alamgir, T. Hu, M. E. Amraoui, Y. Messaddeq, M. Rochette, S. D. Jackson, and A. Fuerbach, "Toward all-fiber supercontinuum spanning the mid-infrared," Optica **4**(10), 1163–1166 (2017).
10. C. R. Petersen, U. Møller, I. Kubat, B. Zhou, S. Dupont, J. Ramsay, T. Benson, S. Sujecki, N. Abdel-Moneim, Z. Tang, D. Furniss, A. Seddon, and O. Bang, "Mid-infrared supercontinuum covering the 1.4–13.3 µm molecular fingerprint region using ultra-high NA chalcogenide step-index fibre," Nat. Photonics **8**(11), 830–834 (2014).
11. A. Lemière, F. Désévédavy, P. Mathey, P. Froidevaux, G. Gadret, J.-C. Jules, C. Aquilina, B. Kibler, P. Béjot, F. Billard, O. Faucher, and F. Smektala, "Mid-infrared supercontinuum generation from 2 to 14um in arsenic- and antimony-free chalcogenide glass fibers," J. Opt. Soc. Am. B **36**(2), A183–A192 (2019).
12. C. Markos, J. C. Travers, A. Abdolvand, B. J. Eggleton, and O. Bang, "Hybrid photonic-crystal fiber," Rev. Mod. Phys. **89**(4), 045003 (2017).
13. M. Cassataro, D. Novoa, M. C. Günendi, N. N. Edavalath, M. H. Frosz, J. C. Travers, and P. S. J. Russell, "Generation of broadband mid-IR and UV light in gas-filled single-ring hollow-core PCF," Opt. Express **25**(7), 7637–7644 (2017).
14. A. I. Adamu, M. S. Habib, C. R. Petersen, J. E. A. Lopez, B. Zhou, A. Schülzgen, M. Bache, R. Amezcua-Correa, O. Bang, and C. Markos, "Deep-UV to Mid-IR Supercontinuum Generation driven by Mid-IR Ultrashort Pulses in a Gas-filled Hollow-core Fiber," Sci. Rep. **9**(1), 4446–4449 (2019).
15. K. L. Corwin, N. R. Newbury, J. M. Dudley, S. Coen, S. A. Diddams, K. Weber, and R. S. Windeler, "Fundamental noise limitations to supercontinuum generation in microstructure fiber," Phys. Rev. Lett. **90**(11), 113904 (2003).
16. A. M. Heidt, J. S. Feehan, J. H. V. Price, and T. Feurer, "Limits of coherent supercontinuum generation in normal dispersion fibers," J. Opt. Soc. Am. B **34**(4), 764–775 (2017).
17. M. Klimczak, B. Siwicki, A. Heidt, and R. Buczyński, "Coherent supercontinuum generation in soft glass photonic crystal fibers," Photonics Res. **5**(6), 710–727 (2017).
18. K. Jiao, J. Yao, Z. Zhao, X. Wang, N. Si, X. Wang, P. Chen, Z. Xue, Y. Tian, B. Zhang, P. Zhang, S. Dai, Q. Nie, and R. Wang, "Mid-infrared flattened supercontinuum generation in all-normal dispersion tellurium chalcogenide fiber," Opt. Express **27**(3), 2036–2043 (2019).
19. Y. Yuan, P. Yang, X. Peng, Z. Cao, S. Ding, N. Zhang, Z. Liu, P. Zhang, X. Wang, and S. Dai, "Ultrabroadband and coherent mid-infrared supercontinuum generation in all-normal dispersion Te-based chalcogenide all-solid microstructured fiber," J. Opt. Soc. Am. B **37**(2), 227–232 (2020).
20. R. Stepien, J. Cimek, D. Pysz, I. Kujawa, M. Klimczak, and R. Buczynski, "Soft glasses for photonic crystal fibers and microstructured optical components," Opt. Eng. **53**(7), 071815 (2014).
21. P. Kaiser, E. a, J. Marcatili, and S. E. Miller, "A new optical fiber," Bell Syst. Tech. J. **52**(2), 265–269 (1973).
22. S. Afshar V., W. Q. Zhang, H. Ebendorff-Heidepriem, and T. M. Monro, "Small core optical waveguides are more nonlinear than expected: experimental confirmation," Opt. Lett. **34**(22), 3577–3579 (2009).
23. L. Fu, B. K. Thomas, and L. Dong, "Efficient supercontinuum generations in silica suspended core fibers," Opt. Express **16**(24), 19629–19642 (2008).
24. I. Shavrin, S. Novotny, and H. Ludvigsen, "Mode excitation and supercontinuum generation in a few-mode suspended-core fiber," Opt. Express **21**(26), 32141–32150 (2013).
25. A. N. Ghosh, M. Klimczak, R. Buczynski, J. M. Dudley, and T. Sylvestre, "Supercontinuum generation in heavy-metal oxide glass based suspended-core photonic crystal fibers," J. Opt. Soc. Am. B **35**(9), 2311–2316 (2018).
26. S. O. Leonov, Y. Wang, V. S. Shiryaev, G. E. Snopatin, B. S. Stepanov, V. G. Plotnichenko, E. Vicentini, A. Gambetta, N. Coluccelli, C. Svelto, P. Laporta, and G. Galzerano, "Coherent mid-infrared supercontinuum generation in tapered suspended-core $As_{39}Se_{61}$ fibers pumped by a few-optical-cycle Cr:ZnSe laser," Opt. Lett. **45**(6), 1346–1349 (2020).
27. E. Coscelli, F. Poli, J. Li, A. Cucinotta, and S. Selleri, "Dispersion engineering of highly nonlinear chalcogenide suspended-core fibers," IEEE Photonics J. **7**(3), 1–8 (2015).

Optical Materials EXPRESS


28. T. Peng, T. Xu, and X. Wang, "Simulation Study on Dispersion Properties of As2S3 Three-Bridge Suspended-Core Fiber," IEEE Access **5**, 17240–17245 (2017).
29. A. Bozolan, C. J. S. de Matos, C. M. B. Cordeiro, E. M. dos Santos, and J. Travers, "Supercontinuum generation in a water-core photonic crystal fiber," Opt. Express **16**(13), 9671–9676 (2008).
30. D. Churin, T. N. Nguyen, K. Kieu, R. A. Norwood, and N. Peyghambarian, "Mid-IR supercontinuum generation in an integrated liquid-core optical fiber filled with CS2," Opt. Mater. Express **3**(9), 1358–1364 (2013).
31. S. Kedenburg, T. Gissibl, T. Steinle, A. Steinmann, and H. Giessen, "Towards integration of a liquid-filled fiber capillary for supercontinuum generation in the 1.2-2.4 μm range," Opt. Express **23**(7), 8281–8289 (2015).
32. V. T. Hoang, R. Kasztelanic, A. Anuszkiewicz, G. Stepniewski, A. Filipkowski, S. Ertman, D. Pysz, T. Wolinski, K. D. Xuan, M. Klimczak, and R. Buczynski, "All-normal dispersion supercontinuum generation in photonic crystal fibers with large hollow cores infiltrated with toluene," Opt. Mater. Express **8**(11), 3568–3582 (2018).
33. V. T. Hoang, R. Kasztelanic, A. Filipkowski, G. Stępniewski, D. Pysz, M. Klimczak, S. Ertman, V. C. Long, T. R. Woliński, M. Trippenbach, K. D. Xuan, M. Śmietana, and R. Buczyński, "Supercontinuum generation in an all-normal dispersion large core photonic crystal fiber infiltrated with carbon tetrachloride," Opt. Mater. Express **9**(5), 2264–2278 (2019).
34. V. T. Hoang, R. Kasztelanic, G. Stępniewski, K. D. Xuan, V. C. Long, M. Trippenbach, M. Klimczak, R. Buczyński, and J. Pniewski, "Femtosecond supercontinuum generation around 1560 nm in hollow-core photonic crystal fibers filled with carbon tetrachloride," Appl. Opt. **59**(12), 3720–3725 (2020).
35. H. L. Van, R. Buczynski, V. C. Long, M. Trippenbach, K. Borzycki, A. N. Manh, and R. Kasztelanic, "Measurement of temperature and concentration influence on the dispersion of fused silica glass photonic crystal fiber infiltrated with water–ethanol mixture," Opt. Commun. **407**, 417–422 (2018).
36. R. Raei, "Supercontinuum generation in organic liquid-liquid core-cladding photonic crystal fiber in visible and near-infrared regions," J. Opt. Soc. Am. B **35**(2), 323–330 (2018).
37. J. Bethge, A. Husakou, F. Mitschke, F. Noack, U. Griebner, G. Steinmeyer, and J. Herrmann, "Two-octave supercontinuum generation in a water-filled photonic crystal fiber," Opt. Express **18**(6), 6230–6240 (2010).
38. K. D. Xuan, L. C. Van, V. C. Long, Q. H. Dinh, L. V. Xuan, M. Trippenbach, and R. Buczynski, "Dispersion characteristics of a suspended-core optical fiber infiltrated with water," Appl. Opt. **56**(4), 1012–1019 (2017).
39. A. Sharafali and K. Nithyanandan, "A theoretical study on the supercontinuum generation in a novel suspended liquid core photonic crystal fiber," Appl. Phys. B **126**(4), 55 (2020).
40. N. Nishizawa and J. Takayanagi, "Octave spanning high-quality supercontinuum generation in all-fiber system," J. Opt. Soc. Am. B **24**(8), 1786–1792 (2007).
41. H. Sotobayashi and K. Kitayama, "325 nm bandwidth supercontinuum generation at 10 Gbit/s using dispersion-flattened and non-decreasing normal dispersion fibre with pulse compression technique," Electron. Lett. **34**(13), 1336–1337 (1998).
42. Y. Liu, Y. Zhao, J. Lyngsø, S. You, W. L. Wilson, H. Tu, and S. A. Boppart, "Suppressing short-term polarization noise and related spectral decoherence in all-normal dispersion fiber supercontinuum generation," J. Lightwave Technol. **33**(9), 1814–1820 (2015).
43. A. M. Heidt, A. Hartung, G. W. Bosman, P. Krok, E. G. Rohwer, H. Schwoerer, and H. Bartelt, "Coherent octave spanning near-infrared and visible supercontinuum generation in all-normal dispersion photonic crystal fibers," Opt. Express **19**(4), 3775–3787 (2011).
44. L. E. Hooper, P. J. Mosley, A. C. Muir, W. J. Wadsworth, and J. C. Knight, "Coherent supercontinuum generation in photonic crystal fiber with all-normal group velocity dispersion," Opt. Express **19**(6), 4902–4907 (2011).
45. S. Rao D. S., D. Engelsholm, I. B. Gonzalo, B. Zhou, P. Bowen, P. M. Moselund, O. Bang, and M. Bache, "Ultra-low-noise supercontinuum generation with a flat near-zero normal dispersion fiber," Opt. Lett. **44**(9), 2216–2219 (2019).
46. I. B. Gonzalo, R. D. Engelsholm, M. P. Sørensen, and O. Bang, "Polarization noise places severe constraints on coherence of all-normal dispersion femtosecond supercontinuum generation," Sci. Rep. **8**(1), 1–13 (2018).
47. C. Huang, M. Liao, W. Bi, X. Li, L. Wang, T. Xue, L. Zhang, D. Chen, L. Hu, Y. Fang, and W. Gao, "Asterisk-shaped microstructured fiber for an octave coherent supercontinuum in a sub-picosecond region," Opt. Lett. **43**(3), 486–489 (2018).
48. A. Hartung, A. M. Heidt, and H. Bartelt, "Pulse-preserving broadband visible supercontinuum generation in all-normal dispersion tapered suspended-core optical fibers," Opt. Express **19**(13), 12275–12283 (2011).
49. #x201C;Lumerical Solutions, Inc.," https://www.lumerical.com/products/mode/.
50. S. Kedenburg, M. Vieweg, T. Gissibl, and H. Giessen, "Linear refractive index and absorption measurements of nonlinear optical liquids in the visible and near-infrared spectral region," Opt. Mater. Express **2**(11), 1588–1611 (2012).
51. D. Pysz, I. Kujawa, R. Stepien, M. Klimczak, A. Filipkowski, M. Franczyk, L. Kociszewski, J. Buzniak, K. Harasny, and R. Buczynski, "Stack and draw fabrication of soft glass microstructured fiber optics," Bull. Pol. Acad. Sci.: Tech. Sci. **62**(4), 667–682 (2014).
52. D. Milam, "Review and assessment of measured values of the nonlinear refractive-index coefficient of fused silica," Appl. Opt. **37**(3), 546–550 (1998).
53. K. J. Blow and D. Wood, "Theoretical description of transient stimulated Raman scattering in optical fibers," IEEE J. Quantum Electron. **25**(12), 2665–2673 (1989).

Optical Materials EXPRESS

54. G. Agrawal, *Nonlinear Fiber Optics*, 5th ed. (Academic Press, 2012).
55. E. Genier, P. Bowen, T. Sylvestre, J. M. Dudley, P. Moselund, and O. Bang, "Amplitude noise and coherence degradation of femtosecond supercontinuum generation in all-normal-dispersion fibers," J. Opt. Soc. Am. B **36**(2), A161–A167 (2019).
56. P. D. Drummond and J. F. Corney, "Quantum noise in optical fibers. I. Stochastic equations," J. Opt. Soc. Am. B **18**(2), 139–152 (2001).
57. F. Poletti and P. Horak, "Dynamics of femtosecond supercontinuum generation in multimode fibers," Opt. Express **17**(8), 6134–6147 (2009).
58. J. M. Dudley and S. Coen, "Coherence properties of supercontinuum spectra generated in photonic crystal and tapered optical fibers," Opt. Lett. **27**(13), 1180–1182 (2002).
59. X. Gu, M. Kimmel, A. P. Shreenath, R. Trebino, J. M. Dudley, S. Coen, and R. S. Windeler, "Experimental studies of the coherence of microstructure-fiber supercontinuum," Opt. Express **11**(21), 2697–2703 (2003).
60. U. Møller and O. Bang, "Intensity noise in normal-pumped picosecond supercontinuum generation, where higher-order Raman lines cross into anomalous dispersion regime," Electron. Lett. **49**(1), 63–65 (2013).